The single-particle distribution function for rapid granular shear flows of smooth inelastic disks

I. Goldhirsch
Department of Fluid Mechanics and Heat Transfer, Faculty of Engineering, Tel-Aviv University, Ramat Aviv, Tel-Aviv 69978, Israel

M-L. Tan
Fluid Dynamics Research Center, James Forrestal Campus, Princeton University, Princeton, New Jersey 08544

(Received 4 October 1994; accepted 1 February 1996)

The velocity distribution function, f_1, for a (linear) shear flow of a system of rigid inelastically colliding disks in a plane is measured by applying a novel algorithm to results of (MD) simulations involving 200 000 particles. The need to consider such a relatively large system is explained. It is found that f_1 is well fitted by an exponent of a second-order polynomial in the norm of the fluctuating velocities with angle-dependent coefficients (which also depend on the density and the granular temperature). Other characterizations of the system studied in this paper are presented as background material. A hitherto unnoticed property of systems with Lees–Edwards boundary conditions has been discovered and its origin is briefly explained. © *1996 American Institute of Physics*. [S1070-6631(96)00306-6]

I. INTRODUCTION

A granular material at high strain rates may be excited so energetically that the frictional contacts between individual grains in it do not endure and a fluidized state in which the grains interact by practically instantaneous collisions emerges.[1–5] The microscopic dynamics of the fluidized granular material ("granular fluid") resembles that of a classical fluid, except for the fact that the collisions in the granular fluid are inelastic. This difference turns out to be a source of numerous phenomena peculiar to granular fluids, such as significant normal stress differences,[1,6–10] spontaneous grain clustering,[11–15] multistability phenomena,[15–17] inelastic collapse,[18–20] and more.[1–5] As a rule granular fluids are generically inhomogeneous.

Despite a very different rheology, many theoretical approaches to the problem of rapid granular flows are heavily based on analogies with the dynamics of molecular fluids. Phenomenological methods,[17,21,22] continuum mechanical,[23] and kinetic theoretical approaches[24–29] are the major means of obtaining constitutive relations for granular materials. When applying kinetic theoretical techniques, the single-particle distribution function, f_1 (and the two-particle distribution function, at collision, in nondilute fluids) is of central importance. This function can, in principle, be extracted from the Boltzmann equation corresponding to the "granular gas" of interest (in the dilute case). Many kinetic studies of granular gases employ conjectures for the form of f_1; usually it is assumed that f_1 has the form of a Gaussian with corrections that are linear in the gradients of the hydrodynamic fields (in parallel to the standard results of the kinetic theory of gases) or a generalized Gaussian.[10,30] The former method fails[26,29] to account for the normal stress differences observed in simulations.[1,7–9] The latter approach does result in normal stress differences that compare well with results of numerical simulations. In another approach to this problem[31] (in which the Enskog correction to the Boltzmann equation is employed), the normal stress differences are attributed to density gradients. In a recent theory[32] it has been shown how a systematic Chapman–Enskog[33] expansion of the Boltzmann equation for granular fluids can be performed, and it has been found that the source of the normal stress differences is the Burnett term.[33] However, this theory is limited to quasielastic systems. Clearly, it is of the utmost importance to elucidate the nature of the single-particle distribution function of granular fluids in an as bias-free and general (e.g., not limited to weak inelasticity) way as possible. We believe that Molecular Dynamics simulations provide the means to achieve this goal. Previous investigations in which this quantity has been studied were limited in accuracy because of insufficient statistics[6–9] or the use of restrictive assumptions such as spatial homogeneity and isotropy.[34]

In the work presented here we consider a two-dimensional system of smooth rigid disks, in a plane, whose collisions are characterized by a single coefficient of normal restitution. A linear velocity profile is achieved by employing the Lees–Edwards boundary conditions.[35] Our main finding is that the single-particle distribution is highly anisotropic (yet quasi-Gaussian in the fluctuating speeds). This finding is related in part to results obtained in Refs. 36 and 37 in which the distribution function of the relative velocities of grains in a vibrated (dense) system has been found to be non-Gaussian and possess power-law tails. Both the latter work and our own reinforce the notion that distributions corresponding to granular matter are different from the familiar distributions encountered in the kinetic theory of molecular systems.

This paper is organized as follows: in Sec. II we present the definition of the system that is studied in this paper. It also provides a description of some general characteristics of the system, such as the temperature, density, and stress profiles and other microscopic and macroscopic characteristics. *In addition, it describes a symmetry breaking effect that shows up in systems with Lees–Edwards boundary condi-*

 1070-6631/96/8(6)/1/12/$10.00

tions and provides a brief explanation of this effect. In Sec. III we present the algorithm that is used to determine the single-particle distribution from numerical data and the results of applying this algorithm to a typical shear flow. In Sec. IV we concentrate on the parametric dependence of the distribution function and present more of its properties. In Sec. V we present a comparison to the theory of Jenkins and Richman and some concluding remarks.

II. SOME CHARACTERISTICS OF THE SIMULATED SYSTEM

A. The model

The simulated system consists of N identical smooth rigid disks of unit mass and diameter σ in a rectangular enclosure of size $L_x \times L_y$. The macroscopic velocity field points in the (streamwise) x direction and varies linearly as a function of y. The Lees–Edwards type of boundary conditions[35] is imposed in the simulations. These conditions were originally employed to study transport properties of simple fluids. Later they were used in simulations of granular systems, e.g., in Refs. 6–9 and 11. These boundary conditions ensure the linearity of the velocity profile (while "saving" the need to formulate a wall boundary condition; cf., e.g., Ref. 38). They correspond to fully periodic boundary conditions applied in the Lagrangian frame for the shear flow[39] (in the y direction). Effectively, one may think of the upper and lower boundaries of the (rectangular) enclosure as moving with velocities equal to $\pm U/2$, respectively, in the x direction. The value of U is fixed as a parameter of the simulation. Since U is the only input quantity whose dimension contains time, fixing the value of U amounts to fixing the unit of time of the problem (also see the beginning of Sec. II B below). The boundary conditions in the x direction are taken to be periodic.

The only allowed interactions in the system are instantaneous collisions of pairs of disks. The collisions occur either between two disks lying within the enclosure or between pairs of disks near opposite boundaries (by the periodicity of the boundary conditions). The velocity of each disk is constant between collisions. The collision process is characterized by a constant coefficient of normal restitution, $\tilde{e}$, with $0<\tilde{e}<1$, i.e. $\mathbf{v}'_{12}\cdot\hat{\mathbf{k}} = -\tilde{e}\mathbf{v}_{12}\cdot\hat{\mathbf{k}}$, where $\mathbf{v}_{12}$ is the relative velocity of two particles (1 and 2) prior to their collision, $\mathbf{v}'_{12}$ is their post-collisional relative velocity and $\hat{\mathbf{k}}$ is the unit vector pointing from the center of particle "1" to that of particle "2" at the time of collision. This collision rule, when combined with the conservation of linear momentum, determines the outcome of the collision. Frictional interactions are not considered in this work.

The initial condition for the simulation is similar to that used in Ref. 11 and it is achieved as follows: a random generator is employed in order to produce a uniform distribution of particles in space with a Gaussian distribution of the fluctuating speeds; care is taken to zero out the small initial total momentum produced by the random generator (by subtracting a fraction $1/N$ of this momentum from the momentum assigned to each particle). The system is then run for some time with a coefficient of restitution of unity to achieve a locally equilibrated state (with shear) and then the inelastic collisions are turned on. The numerical method employed in the simulation is the highly efficient "event-driven" algorithm.[40]

B. Some characteristics of the simulated system

The simulation of the system described in Sec. II A shows that the system reaches a statistical steady state in a (practically) finite time. In the simulation, a state of the system is considered to be steady if several statistical characteristics, to be described below, are time independent to within numerical accuracy. It is important to stress that sheared granular systems possess multiple steady states,[15,16] the character of each of which depends on the initial condition of the system and the transient stage of its evolution; here we limit our consideration to the steady state obtained by the procedure described in Sec. II A. The parameters characterizing the system at hand are the coefficient of restitution, $\tilde{e}$, the total number of particles, N, the values of U, L_x, L_y and the diameter, σ, of the disks. A useful dimensionless quantity is the system's average solid fraction, $\bar{\nu}$, defined as $\pi N\sigma^2/4L_xL_y$. The average shear rate, γ, is defined as U/L_y (this is the only time scale determined by the input). Notice that the values of N, $\bar{\nu}$, L_x, and L_y determine σ.

An elastic system subject to the Lees–Edwards boundary conditions heats up monotonically while remaining in a state whose temperature, density, and macroscopic velocity gradient are spatially uniform. The inelastic system, on the other hand, has an internal energy sink due to the inelastic collisions; hence it does, when subject to the same boundary conditions, reach a state having a steady average granular temperature that is determined by the balance between the rate of energy pumped into the system by the shearing and the rate at which energy is dissipated by the collisions. We have found that the steady average granular temperature, $\bar{T}$, which is defined as one-half the average of the square of the fluctuating velocities of all particles in the system, can be closely fitted by the following empirical relation:

$$\bar{T} = A\,\frac{\gamma^2\sigma^2}{\bar{\nu}^2}\left(\frac{1}{1-\tilde{e}^2}+B\right). \tag{1}$$

Here $A \simeq 0.080$ and $B \simeq -0.54$ are dimensionless constants. The ratio $\sigma/\bar{\nu}$ is proportional to the mean-free path in a homogeneous system of solid fraction $\bar{\nu}$. Figure 1 illustrates this relationship by comparing the values of $\bar{T}$ in systems characterized by different values of $\tilde{e}$. The straight line through the data points in Fig. 1 is the dilute limit form of the relationship between $\bar{T}$ and $\tilde{e}$ as derived by Jenkins and Richman in Ref. 10. Following Eq. (70) and Eq. (71) in Ref. 10, this dilute limit relationship is

$$\bar{T} = \frac{\pi}{(1+\tilde{e})^2(7-3\tilde{e})^2}\,\frac{\gamma^2\sigma^2}{\bar{\nu}^2}\left(\frac{1}{1-\tilde{e}}-\frac{7}{16}\right). \tag{2}$$

It is easy to check that Eq. (2) and Eq. (1) yield close results as $\tilde{e}$ approaches unity. It should be noted that the theory in Ref. 10 considers a spatially uniform and time-independent shear flow, whereas the actual flow is highly nonuniform and it exhibits time-dependent microstructures. In view of this

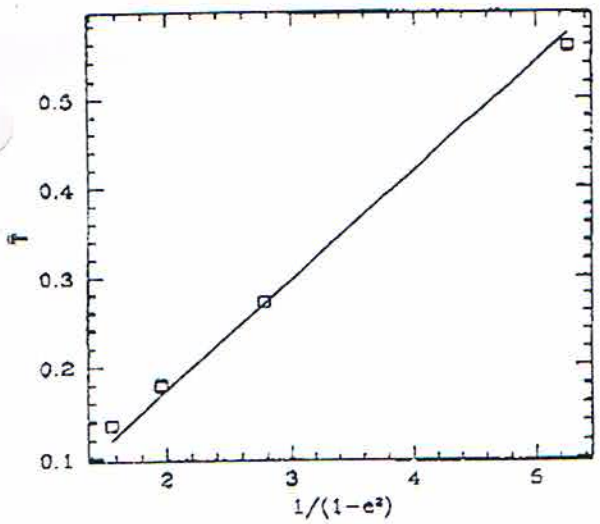

FIG. 1. The average temperature, $\bar{T}$, vs $1/(1-\bar{e}^2)$. The data are obtained from systems whose parameters other than $\bar{e}$ are given by $N=200\,000$, $U=100$, $L_x=L_y=1$, and $\bar{\nu}=0.05$. The solid line through the data points is the prediction of the generalized Gaussian theory of Jenkins and Richman.

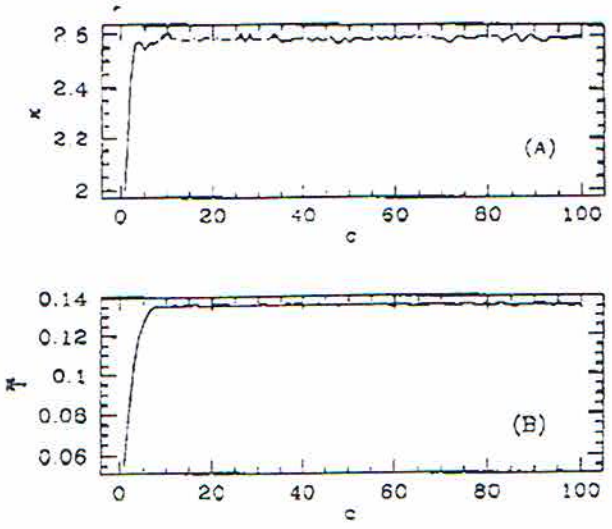

FIG. 2. Panel (a): the global flatness of the distribution of fluctuating velocities for System I versus the accumulated number of collisions per particle, c, in the system. Panel (b): the average temperature as a function of c.

fact, the agreement of the result for the average temperature with the predictions of Ref. 10 is somewhat surprising. It would be interesting to find out which other average quantities are unaffected by the existence of microstructures (and why).

In the rest of this section we wish to present a detailed description of our findings for a specific, though typical, sheared system. The parameters of the system that we have chosen are given by $\bar{e}=0.6$, $N=200\,000$, $U=100$, $L_x=L_y=1$, and $\bar{\nu}=0.05$. This system is dilute and highly inelastic and will henceforth be referred to as System I.

The manner in which the various macrofields are computed from data obtained from the simulation is as follows. The density field, $\rho(\mathbf{r})$, is defined (in a rather usual way) by partitioning the flow domain into an array of 100×100 cells and counting the number of particles in each cell (the particles are assumed to have unit mass). The position $\mathbf{r}$ is taken to be the position vector of the center of the cell. The macroscopic velocity field, $\mathbf{V}(\mathbf{r})$, is obtained by computing the ratio of the total momentum to the total mass in each cell. The granular temperature (or fluctuating energy density) in a cell is defined as $T(\mathbf{r})\equiv\frac{1}{2}\langle[\mathbf{v}-\mathbf{V}(\mathbf{r})]^2\rangle$, where $\mathbf{v}$ denotes the velocity of a particle in the cell and $\langle\cdots\rangle$ denotes an average over all particles in the cell.

Next, we define the stress tensor, $\tau(\mathbf{r})$, which is a sum of a "kinetic" contribution that accounts for the transport of momentum as the particles move and a "collisional" contribution that accounts for the transfer of momentum as the particles collide.[9,8,11] For a given configuration, the $\alpha\beta$ component of the average kinetic stress tensor is given by $\tau^{(k)}_{\alpha\beta}(\mathbf{r})=\rho(\mathbf{r})\langle v'_\alpha v'_\beta\rangle$, where $v'_\alpha=v_\alpha-V_\alpha(\mathbf{r})$. The product $\langle v'_\alpha v'_\beta\rangle$ is computed using the identity $\langle v'_\alpha v'_\beta\rangle=\langle v_\alpha v_\beta\rangle-\langle v_\alpha\rangle\langle v_\beta\rangle$. The collisional stress tensor[1,33] is computed as follows. Let $\mathbf{J}$ denote the impulse transfer in a binary collision (i.e., the magnitude of the change in the momentum of each of the colliding particles), $\hat{\mathbf{k}}$ a unit vector pointing from the center of one of the colliding particles to the center of the particle it collides with. The collisional contribution to the stress tensor, $\tau^{(c)}(\mathbf{r})$, is $\tau_c=\sigma/At\Sigma_{\text{collisions}}\mathbf{J}\hat{\mathbf{k}}$, where the sum is over collisions occurring within a cell of area A in a time interval t (i.e., an average of the dyadic product $\mathbf{J}\hat{\mathbf{k}}$ over these collisions). The total stress tensor is then given by $\tau(\mathbf{r})\equiv\tau^{(k)}(\mathbf{r})+\tau^{(c)}(\mathbf{r})$.

The global average granular temperature, $\bar{T}$ (mentioned above), is defined as the average of $T(\mathbf{r})$ over all cells in the system. The variation of $\bar{T}$ with time can be used to gauge the convergence of the system to a steady state, since $\bar{T}$

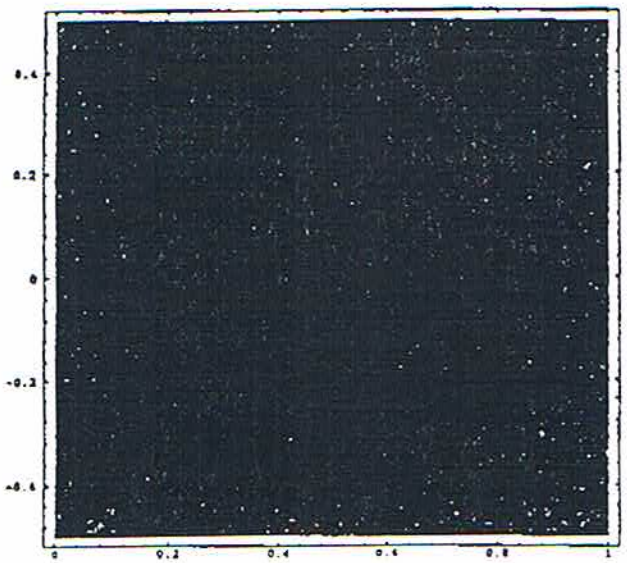

FIG. 3. The density field for System I at a time corresponding to 100 collisions per particle following the initial condition. The shade code is lighter gray for higher densities and darker for lower densities.

pls remove the word 'is'

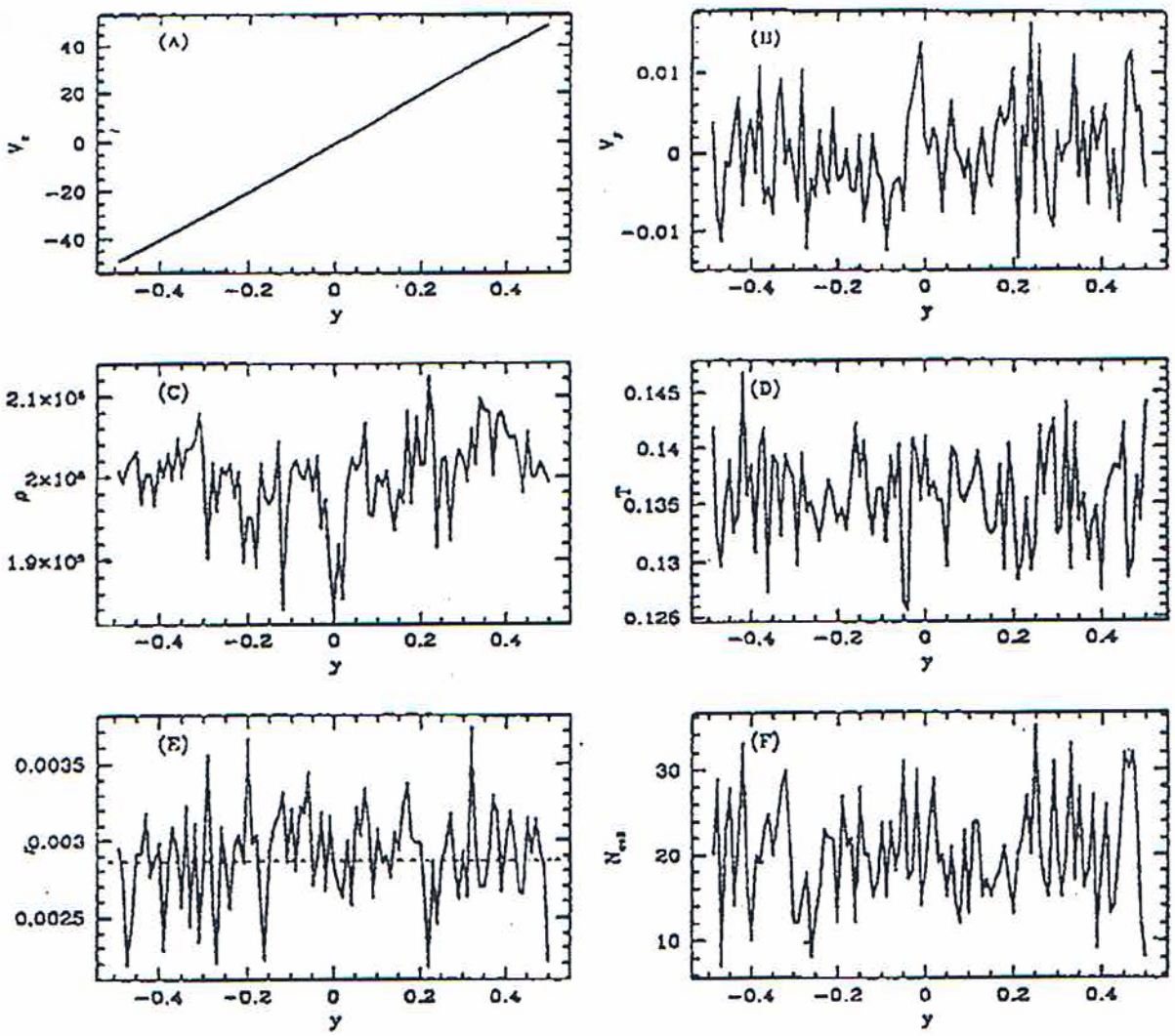

FIG. 4. Streamwise-averaged flow properties for System I: (a) V_x; (b) V_y; (c) density, ρ; (d) temperature, T; (e) rms deviation, r, from the cell center of x coordinates of particles in a cell versus the position of the cell in a spanwise column (the dashed line corresponds to the value for a homogeneous distribution of particles); (f) the number of particles in a cell, N_{cell} versus the cell position in the same column as in (e). Notice that all profiles are essentially uniform, the relative fluctuations being very small.

approaches, and then fluctuates around, a steady value when this occurs (cf. Fig. 2). The measure of time in Fig. 2 is the accumulated number of collisions per particle, denoted by c. Another useful global diagnostic is the flatness (kurtosis), κ, of the distribution of fluctuating velocities, which is defined as $\kappa = \overline{v'^4}/\overline{v'^2}^2$, where the overbar denotes an average over all particles in the system. A plot of κ as a function of c for System I as it is driven from its initial condition to a statistically steady state is shown in Fig. 2. The value of κ at $c=0$ is 2, as expected for a Maxwellian distribution; the steady-state value, which is achieved after about ten collisions per particle, is significantly different from 2.

A shaded density contour plot at a time corresponding to the lapse of 100 collisions per particle is shown in Fig. 3. The brightest shade in this plot corresponds to a value of the density at approximately 80% of the full range of densities observed in the flow and the darkest shade to 20% of the this range. The intermediate grey shades are "equally spaced." The extreme values of the density are approximately ±50% of the average value. The values of $\overline{T}$ and the flatness, κ, are statistically stationary at this time, and thus the flow is assumed to have converged to a statistically stationary state. The flow is really not locally stationary in time: an examination of a movie depicting the dynamics of the system or of consecutive density plots reveals that clusters of particles form continually and then merge or break up as they collide with each other.[16] Every single snapshot, such as the the density field presented in Fig. 3, reveals that the density is highly inhomogeneous. Despite the spatiotemporal variations in the density, the profile of the streamwise velocity field remains linear across the domain, as shown in Fig. 4(a), at all times. In addition, by computing the corresponding vorticity

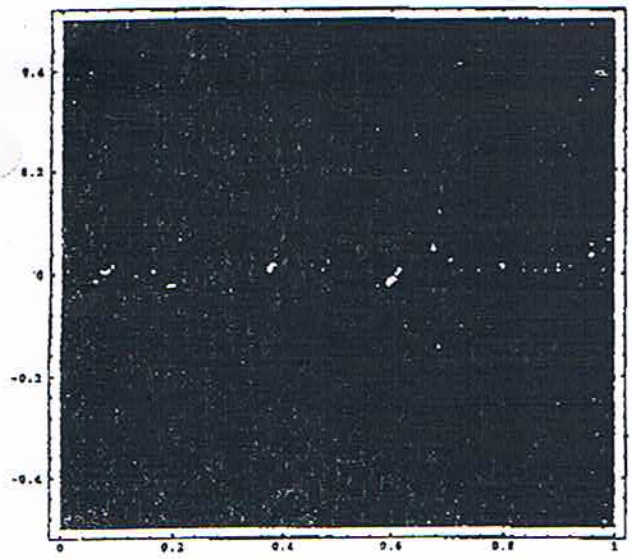

FIG. 5. The collisional pressure field for System I at a time corresponding to 100 collisions per particle following the initial condition. The shade code is lighter gray for higher pressures and darker for lower pressures. Notice the brighter strip near the centerline.

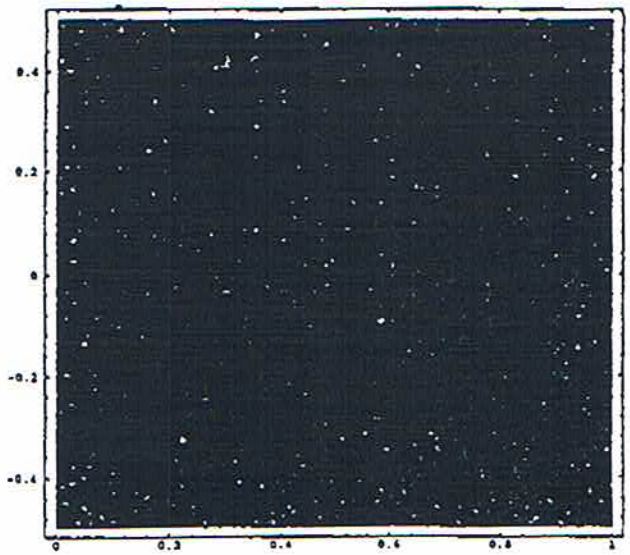

FIG. 6. The kinetic pressure field for System I at a time corresponding to 100 collisions per particle following the initial condition. The shade code is lighter gray for higher pressures and darker for lower pressures.

field, we have found that the velocity field corresponds everywhere to a highly uniform shear field. Some other streamwise-averaged properties, such as the temperature and number density profiles, are shown in Fig. 4. These profiles show variations characterized by distinct length scales on an essentially flat background.

Another quantity, depicted in Fig. 4(c), is a measure of the uniformity of the distribution of the particles in the cells defined in the coarse-graining partition of the flow domain. This is the root-mean-square deviation, r, of the x coordinates of the particles in a cell from the geometric center of the cell and it is defined as $\sqrt{(1/n)\Sigma_i(x_i-x_0)^2}$, where n is the number of particles in the cell, x_i is the x coordinate of the ith particle in the cell, x_0 is the x coordinate of the center of the cell, and i is taken over all particles in the cell. The value of r for a uniform distribution is $(\sqrt{1/12})l_x$, where l_x is the horizontal dimension of the cell. The variation of r along a vertical (i.e., spanwise) column of cells is shown in Fig. 4(e) and the variation of the number of particles in a cell in the same column is shown in Fig. 4(f). These figures show that, despite the comparatively large fluctuations in the *number of particles* per cell among the cells, r almost never deviates by more than 10% from its homogeneous value. This fact indicates that the chosen scale of the coarse graining cell is just right: large enough to contain a significant number of particles yet small enough for the density to be practically uniform in the cell.

The collisional and kinetic pressure fields for System I at the same time as the corresponding to the density field are shown in Fig. 5 and Fig. 6, respectively. The grey scale resolution in these figures is the same as in Fig. 3. The collisional and kinetic pressures are defined as one-half the traces of the corresponding stress tensors. A correlation analysis of the data reveals that regions of higher density correspond to lower temperatures and pressures. This fact can be explained as being a result of the competition between collisional cooling[12,13] (a mechanism that has been shown to lead to the emergence of clusters[15,16] of low granular temperature and relatively high density) and heating by the shear flow. The combined action of the two is responsible for arresting the clustering process when the value of the density reaches a certain ("compromise") level, a similar statement holding for the temperature.

Note the bright spots (higher collisional pressures) near the centerline of Fig. 5. This phenomenon is a result of a *symmetry breaking effect* (characterizing Lees–Edwards systems) that is explained below. The density distribution and the (thermal) distribution of fluctuating velocities (as well as of the relative velocities of colliding particles) are essentially independent of the vertical distance, $|y|$, from the centerline—as expected in a Lees–Edwards system. This means that the mean-free time (i.e., the time between consecutive collisions of a particle) is practically independent of the y coordinate. The particles near the centerline ($y=0$) have near zero average velocity, their speeds are mainly thermal and the directions of their velocities are nearly isotropic. The mean-free path near the centerline is small with respect to the system size (and its magnitude is well approximated by the standard result of kinetic theory ($1/n\sigma_t$), where n is the number density and σ_t is the total collisional cross section). In contrast, for large enough values of $|y|$ the velocity of a typical particle is composed of a large average part and a relatively small (the same as for $y=0$) thermal part (hence it is "supersonic"). Thus particles situated far from the centerline move rapidly (and essentially in the $\pm x$ direction) and their mean-free paths (performed during a mean-free time, which is practically the same at all values of y) are far larger

$\sqrt{1/12}$ (see manuscript)

than those corresponding to particles near the centerline. These rapid particles can traverse the entire computational enclosure without experiencing a collision. This conclusion is corroborated by our numerical findings. It follows that while the system near the centerline can be considered to be fully macroscopic (i.e., system size far larger than the mean-free path), this is not the case far enough from the centerline. This symmetry breakdown of the Lees–Edwards boundary conditions is not peculiar to granular systems alone; we have checked that it shows up in elastic systems as well. There, since the system heats up in time, the whole system becomes subsonic after some time and the effect disappears. In a granular system the average temperature reaches a steady value and the above effect persists at all times. A detailed analysis of this symmetry breaking effect is relegated to another publication.

III. DETERMINATION OF THE SINGLE-PARTICLE DISTRIBUTION FUNCTION

In this section, we present a new algorithm that determines the single-particle distribution function from data obtained in the simulations. This function is denoted by $f_1(\mathbf{r},\mathbf{v};t)$, where $\mathbf{r}$ and $\mathbf{v}$ denote the position and fluctuating velocity, respectively, and t denotes the time. The algorithm is based on the observation that a monotonic integral of a noisy positive-definite-quantity is comparatively less susceptible to distortion by noise and poor statistics than the quantity itself and it may thus be fitted more readily by smooth functions. This integral is constructed from data, then fitted to an appropriate smooth function, which is subsequently differentiated. The resulting function is still smooth and can be fitted again to a different functional form that is more convenient than the one used in the first fit (i.e., an exponential of a function; cf. below).

A. The algorithm

Since the flow is statistically stationary in time—$f_1(\mathbf{r},\mathbf{v};t)$ is not an explicit function of time. It is well known that the single-particle distribution function can be represented as $f_1(\mathbf{r},\mathbf{v})=\langle\Sigma_{i=1}^{N}\delta(\mathbf{r}-\mathbf{r}_i)\delta(\mathbf{v}-\mathbf{v}_i)\rangle$, where $\mathbf{r}_i$ and $\mathbf{v}_i$ are the position and velocity of the ith particle and $\langle\cdots\rangle$ denotes an average over a statistical ensemble of systems characterized by the same parameters as the one of interest (in contrast to Sec. II B in which $\langle\cdots\rangle$ denotes an average over particles in a cell). The function f_1 obeys the normalization $\int_{\mathbf{V}} f_1(\mathbf{r},\mathbf{v})d\mathbf{v}=\langle\Sigma_{i=1}^{N}\delta(\mathbf{r}-\mathbf{r}_i)\rangle=\rho(\mathbf{r})$ and $\int_{\mathbf{r}}\int_{\mathbf{V}} f_1(\mathbf{r},\mathbf{v})d\mathbf{v}\,d\mathbf{r}=N$, where $\rho(\mathbf{r})$ is the number density; the subscript $\mathbf{V}$ denotes integration over velocity and the subscript $\mathbf{r}$ denotes integration over the coordinates. Since the mean velocity field corresponds to linear shear, it is reasonable to assume that f_1 depends on the position $\mathbf{r}$ through the local density, $\rho(\mathbf{r})$, the local temperature, $T(\mathbf{r})$, and the local mean velocity, $\mathbf{V}(\mathbf{r})$. Also, f_1 should depend on $\mathbf{V}(\mathbf{r})$ through the difference $\mathbf{v}-\mathbf{V}(\mathbf{r})$. All in all, we assume that f_1 can be written as $f_1[\rho(\mathbf{r}),T(\mathbf{r}),\upsilon]=f^{(1)}[\rho(\mathbf{r}),T(\mathbf{r}),\mathbf{v}-\mathbf{V}(\mathbf{r})]$. Notice that $f^{(1)}$ is assumed not to depend *explicitly* on the gradients of the velocity, temperature, and density fields. This does not imply that $f^{(1)}$ does not depend on these gradients; rather, it is assumed (and corroborated *a posteriori* by the numerical results) that in the steady state considered here there is a one-to-one correspondence between the values of the hydrodynamic fields and their gradients, hence $f^{(1)}$ depends implicitly on the latter. Since the values of the density and temperature are taken to determine the values of their gradients, a strong correlation between the distributions of these fields and their gradients is implied. The physical basis for this is the particular structure of the considered flow: A point in the flow is either inside a cluster or a dilute region, or it is at the "interface" between a cluster and the dilute region immediately surrounding it. In each case, the density and temperature at a given point as well as their gradients at that point are (practically) determined by the type of environment in which this point resides. One of these gradients, the shear rate, is found to be highly uniform in the system (cf. Sec. II B) and it is considered to be a fixed parameter of the system, γ. Clearly $f^{(1)}$ depends also on the other (global) parameters defining the system; this dependence is not explicitly spelled out for the sake of notational simplicity.

It follows that $f^{(1)}$ can be determined, for given values of the density $\rho=\rho_0$ and temperature $T=T_0$, by collecting statistics in regions of the flow whose density and temperature are simultaneously ρ_0 and T_0, respectively. In practice, one has to define small windows in the density and temperature that are centered around predetermined values of these quantities so that statistically significant results can be obtained. The sampling procedure consists of the following steps: (1) The system is divided into cells and the temperature and density in each cell is determined, as explained in Sec. II B; (2) the cells whose temperature and density lie within the predetermined windows are identified; (3) a process of "binning" the fluctuating velocities of the particles in these cells, in terms of the norms and polar angles (relative to the streamwise direction) of these velocities, is performed. The information obtained from the binning process is used as described below.

Let Ω_{ρ_0,T_0} denote the total area of the cells whose density lies within a window around ρ_0 and T_0. Let $S(\rho_0,T_0)$ denote this set of cells. Also let $\hat{f}^{(1)}$ denote the numerical approximation of $f^{(1)}$ given by

$$\hat{f}^{(1)}[\rho_0,T_0,\mathbf{v}-\mathbf{V}(\mathbf{r})]=\frac{1}{\Omega_{\rho_0,T_0}}\int_{S(\rho_0,T_0)} f^{(1)} \times[\rho(\mathbf{r}),T(\mathbf{r}),\mathbf{v}-\mathbf{V}(\mathbf{r})]d\mathbf{r}, \quad (3)$$

$$=\left\langle\frac{1}{\Omega_{\rho_0,T_0}}\int_{S(\rho_0,T_0)}\sum_{i=1}^{N}\delta(\mathbf{r}-\mathbf{r}_i) \times\delta(\mathbf{v}-\mathbf{v}_i)d\mathbf{r}\right\rangle, \quad (4)$$

$$=\left\langle\frac{1}{\Omega_{\rho_0,T_0}}\sum_{i\in S(\rho_0,T_0)}\delta(\mathbf{v}-\mathbf{v}_i)\right\rangle. \quad (5)$$

The integrals in Eq. (3) and Eq. (4) extend over $S(\rho_0,T_0)$, as denoted above. As mentioned, $\langle\cdots\rangle$ denotes an average over an ensemble of realizations; in practice it means averaging over a series of snapshots of the system. The area Ω_{ρ_0,T_0} is

included in the ensemble average because it may vary from one system to another in the ensemble. For notational simplicity, we drop the subscript 0 in ρ_0 and in T_0 and introduce $N_{\rho,T}/\Omega_{\rho,T}$, where $N_{\rho,T}$ is the total number of particles in ...s of density ρ and temperature T. For narrow enough windows it follows that

$$\hat{f}^{(1)}[\rho,T,\mathbf{v}-\mathbf{V}(\mathbf{r})]=\rho\left\langle\frac{1}{N_{\rho,T}}\sum_{i\in S(\rho,T)}\delta(\mathbf{v}-\mathbf{v}_i)\right\rangle. \tag{6}$$

Let $\mathbf{v}_i'=\mathbf{v}_i-\mathbf{V}(\mathbf{r}_i)$ denote the fluctuating component of the velocity of particle i. It follows that $\hat{f}^{(1)}$ can be rewritten as follows:

$$\hat{f}^{(1)}(\rho,T,\mathbf{v})=\rho\left\langle\frac{1}{N_{\rho,T}}\sum_{i\in S(\rho,T)}\delta(\mathbf{v}-\mathbf{v}_i')\right\rangle. \tag{7}$$

It is convenient to define

$$\tilde{f}^{(1)}(\rho,T,\mathbf{v})\equiv\left\langle\frac{1}{N_{\rho,T}}\sum_{i\in S(\rho,T)}\delta(\mathbf{v}-\mathbf{v}_i')\right\rangle\equiv\frac{\hat{f}^{(1)}(\rho,T,\mathbf{v})}{\rho}. \tag{8}$$

Notice that $\tilde{f}^{(1)}$ is normalized to unity. The cumulative distribution function for a two-dimensional system is defined by

$$h(v,\theta)\equiv\int_{v'=0}^{v}\int_{\theta'=0}^{\theta}\tilde{f}^{(1)}(v',\theta')v'\,dv'\,d\theta', \tag{9}$$

where we have used polar coordinates for $\mathbf{v}$, and the dependence on ρ and T is implicitly assumed for notational convenience. Clearly, $h(v,\theta)$ is proportional to the number of particles whose fluctuating velocity has a magnitude less than v and a direction angle between 0 and θ. Obtaining this ...ntity from the data is merely a matter of counting. Since ...e normalization for $\tilde{f}^{(1)}$ is $\int_{v'=0}^{\infty}\int_{\theta'=0}^{2\pi}\tilde{f}^{(1)}\times(v',\theta')v'\,dv'\,d\theta'=1$ it follows that $h(\infty,2\pi)=1$. Two further observations may be made here: the derivative of $h(v,\theta)$ with respect to θ, $h_\theta(v,\theta)=\int_{v'=0}^{v}\tilde{f}^{(1)}(v',\theta)v'\,dv'$ is periodic in θ since $\tilde{f}^{(1)}(v,\theta)$ is periodic in θ. Also, it is obvious that for small enough values of v, the function h_θ is given, to leading order in v, by $v^2\times$(a function of θ). We make use of the first observation to write h_θ as a Fourier series:

$$h_\theta(v,\theta)=c_0(v)+\sum_{n\neq0}c_n(v)\exp(in\theta). \tag{10}$$

Integration of Eq. (10) with respect to θ yields

$$h(v,\theta)=\int_{\theta'=0}^{\theta}h_\theta'\,d\theta'=\sum_{n\neq0}\frac{i}{n}c_n(v)+c_0(v)\theta+\sum_{n\neq0}c_n(v)\frac{\exp(in\theta)}{in}. \tag{11}$$

Thus $h(v,\theta)$ may be expressed as a sum of terms that are independent of θ, a term that is linear in θ and terms that are periodic in θ. Notice that by Eq. (9), $h(v,0)=0$ and by Eq. (11), $h(v,2\pi)-h(v,0)=h(v,2\pi)=2\pi c_0(v)$. It follows from Eq. (9) and Eq. (11) that the double derivative of h with respect to the angle θ and the velocity v can be expressed as follows: $h_{v\theta}(v,\theta)=v\tilde{f}^{(1)}(v,\theta)=\varphi_v(v)+\psi_{\theta v}(\theta,v)$, where

$$\psi(\theta,v)\equiv\sum_{n\neq0}c_n(v)\frac{\exp(in\theta)}{in}, \tag{12}$$

$$\varphi(v)\equiv\frac{h(2\pi,v)}{2\pi}=c_0(v). \tag{13}$$

Once $h(v,\theta)$ is obtained from data (by counting, as mentioned), $\varphi(v)$ may then be computed using Eq. (13), and $\psi(\theta,v)$ can be obtained from the identity

$$\psi(\theta,v)=h(v,\theta)-\frac{1}{2\pi}\int_{\theta=0}^{\theta=2\pi}h(v,\theta)d\theta+(\pi-\theta)\varphi(v), \tag{14}$$

which follows from Eqs. (11) and (12) by using the fact that the average of the last term on the rhs of Eq. (11) over the full range of angles vanishes. It is easy to check that ψ as given by Eq. (14) is periodic in θ, as it should be. Once $h(v,\theta)$ is measured, we can use the above expressions to obtain $\varphi(v)$ and $\psi(v,\theta)$ whence $\hat{f}^{(1)}(v,\theta)$ is deduced.

We have found, on the basis of the data we obtained from the simulations, that the functions $\varphi(v)$ and $\psi(\theta,v)$ can be closely fitted by the functions $\varphi^*(v)$ and $\psi^*(\theta,v)$, respectively, where

$$\varphi^*(v)\equiv\frac{1-\exp[-J(v)]}{2\pi}, \tag{15}$$

$$\psi^*(v,\theta)\equiv\sum_{p=1}^{4}A_p(v)\sin[2p(\theta+\beta)], \tag{16}$$

with

$$J(v)\equiv\sum_{m=2}^{4}a_m v^m, \tag{17}$$

$$A_p(v)\equiv\alpha_p\{1-\exp[-Q_p(v)]\}, \tag{18}$$

$$Q_p(v)\equiv\sum_{m=2}^{6}d_{pm}v^m, \tag{19}$$

where $J(v)$ is of quartic order in v, $Q_p(v)$ are polynomials of sixth order in v, and α_p is the asymptotic value of $A_p(v)$ for large v. The reason only even multiples of θ appear in Eq. (16) is the "π rotation" symmetry obeyed by the shear flow. The expansions in Eq. (17) and Eq. (19) start with $m=2$ since (as mentioned above) h_θ is proportional to v^2 for small values of v. The number of terms in the truncated sine series in Eq. (16) is determined by requiring the fit to be accurate to within 1% for large values of v and to within 5% for small values of v. The error tolerance level is relaxed for small values of v because the numerical data for these values tend to be noiser—a fact that is to be expected since the cumulative sampling technique used in the algorithm improves the statistics at moderate values of v but is not as effective for small v. For large v, the accuracy can be maintained since the numerical data tend to an asymptotic functional form.

The value of the phase β is found to depend on ρ, T, and e. Graphs of $h(v,\theta)$ vs v for several values of θ are shown in Fig. 7. A graph of $J(v)$ and its fit, Eq. (17), is shown in Fig. 8, and graphs of $\psi(v,\theta)$ along with the fit, Eq. (16), is

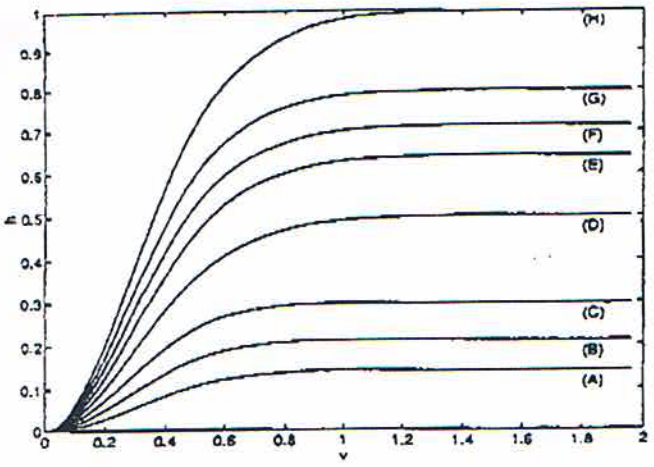

FIG. 7. The cumulative distribution function $h(v,\theta)$ vs v for values of $\theta=n\pi/4$, $n=1,2,\ldots,8$, corresponding to the curves (a)–(h), respectively. Notice that $h(v,\theta)$ is smooth and that it increases monotonically with v and θ. The data correspond to System I, and the windows in ρ and T are $(2.8\pm0.2)\times10^3$/unit area and 0.11 ± 0.0075, respectively. The average temperature, $\bar{T}$, for the system is 0.15.

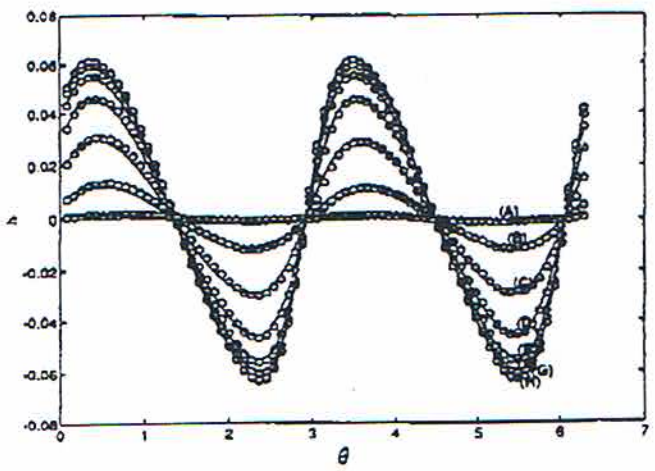

FIG. 9. The periodic part, $\psi(v,\theta)$, of the function $h(v,\theta)$ shown in Fig. 7, versus θ for the values of v: 0.2, 0.4, 0.6, 0.8, 1.2, 2.0, corresponding to the sets of curves (a)–(f), respectively. The points correspond to the data and solid curves are given by Eq. (16). Notice that $\psi(v,\theta)$ crosses the θ axis at the same values of θ for different v.

shown in Fig. 9. These graphs are derived from data taken from a time series of 20 configurations of System I sampled at times separated by intervals corresponding to the accumulation of one collision per particle in the system.

Next, a fit to $h_{v\theta}$ is obtained by differentiating the functions in Eq. (15) and in Eq. (16). The result, which is written as $h^*_{v\theta}(v,\theta)=\varphi^*_v(v)+\psi^*_{v\theta}(\theta,v)$, is referred to below as the "once-fitted" approximation of the distribution function; that is, we define $\hat{f}^{(1)*}\equiv h^*_{v\theta}(v,\theta)/v$, where the once-starred quantities refer to results of the fitting procedure. The next step is to fit the function $-\log(\hat{f}^{(1)*})$ by another analytic function so as to obtain a form that is similar to those used in the kinetic theory of gases (i.e., one that is the exponential function of an expression in the velocity). We have found

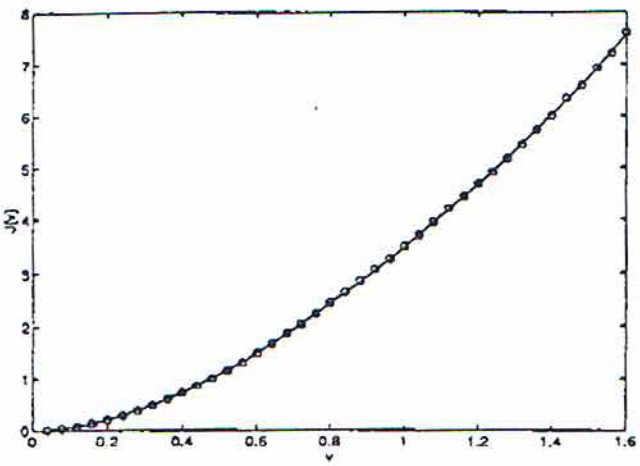

FIG. 8. The $J(v)$ (points) and its fit (solid line) given by Eq. (17). The cumulative distribution, $h(v,\theta)$, from which this graph is derived, is shown in Fig. 7.

that the following expression furnishes a close fit to $-\log(\hat{f}^{(1)*})$: $-\log(\hat{f}^{(1)**})=b^{(0)}(\theta)+b^{(1)}(\theta)v+b^{(2)}(\theta)v^2$, where the coefficients $b^{(i)}$, $i=0,1,2$, are functions of θ. The double-star superscript in $\hat{f}^{(1)**}$ indicates that this function is a "second fit" to the "first fit," $\hat{f}^{(1)*}$. The "twice-fitted" approximation to the single-particle distribution function is thus

$$\hat{f}^{(1)}(v,\theta;\rho,T,\tilde{e})\simeq\rho\hat{f}^{(1)**}=\rho\exp[-b^{(0)}(\theta;\rho,T,\tilde{e})-b^{(1)}(\theta;\rho,T,\tilde{e})v-b^{(2)}\times(\theta;\rho,T,\tilde{e})v^2], \tag{20}$$

in which we have made explicit the dependence on the macrofields and the parameters of the system. As $\hat{f}^{(1)}$ is periodic in θ with period π, so are the functions $b^{(0)}$, $b^{(1)}$, and $b^{(2)}$. It follows that these coefficients can be expanded in a sine series:

$$b^{(i)*}(\theta;\rho,T,\tilde{e})=b_0^{(i)*}(\rho,T,\tilde{e})+\sum_{j=1}^{6}b_{2j}^{(i)*}(\rho,T,\tilde{e})\sin\{2j[\theta+\epsilon_{2j}\times(\rho,T,\tilde{e})]\},\quad i=0,1,2. \tag{21}$$

In the above expansion, the amplitudes $b_{2j}^{(i)*}$ and phase shifts ϵ_{2j} depend on ρ, T, and $\tilde{e}$. Note that the set of phase shifts ϵ_{2j} is the same for all $b^{(i)*}$, $i=0,1,2$, as expected from the "rotation by π" symmetry of the flow. A graph of ϵ_{2j} vs T at fixed ρ is shown in Fig. 10. As indicated in Eq. (21), the truncation of the series to only six sine harmonics is sufficient to reproduce the $b^{(i)}$'s accurately. The quality of the fit $b^{(i)*}$ to the corresponding $b^{(i)}$ that were obtained from the data is demonstrated in Fig. 11. The zeroth-order amplitudes, $b_0^{(i)*}$, of this fit, i.e., the mean values of $b^{(i)*}$, are shown versus T at fixed ρ in Fig. 12. The points shown are nondimensionalized, as explained in the figure caption. It is useful

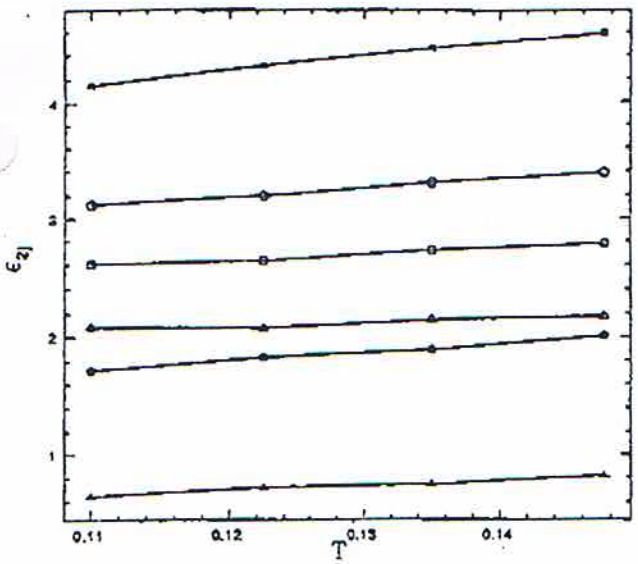

FIG. 10. Phase shifts ϵ_{2j}, $j=1,\ldots,6$, corresponding to ▲, ■, ◆, △, □, and ◇, respectively, versus T for $\rho=2.8\times10^5$.

to note that the corresponding graph for an elastic system in a state of equilibrium would be given by $2T\tilde{b}_0^{(2)}=1$ and $\sqrt{2T}\tilde{b}_0^{(1)}=0$.

An additional assessment of the quality of these fits can

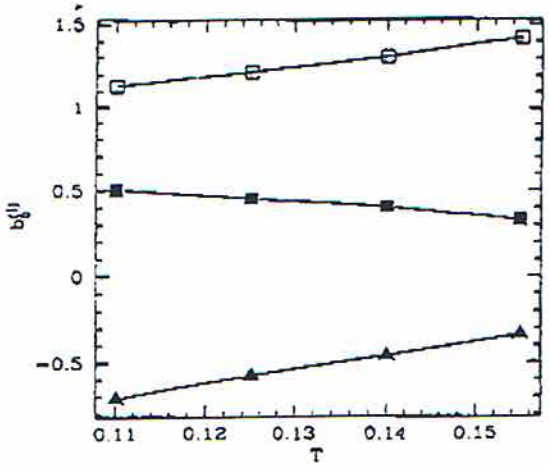

FIG. 12. Nondimensionalized zeroth-order amplitudes, $b_0^{(0)}$, $\sqrt{2T}b_0^{(1)}$, and $2Tb_0^{(2)}$, corresponding to ▲, ■, and □, respectively, versus T for $\rho=2.8\times10^5$.

be obtained by comparing the kinetic stresses calculated by using $\tilde{f}^{(1)*}$ and $\tilde{f}^{(1)**}$ Let

$$\tau^{(k)*}(\rho,T)=\begin{pmatrix} \int v^3\cos^2\theta\tilde{f}^{(1)*}(v,\theta)dv\,d\theta & \int v^3\cos\theta\sin\theta\tilde{f}^{(1)*}(v,\theta)dv\,d\theta \\ \int v^3\cos\theta\sin\theta\tilde{f}^{(1)*}(v,\theta)dv\,d\theta & \int v^3\sin^2\theta\tilde{f}^{(1)*}(v,\theta)dv\,d\theta \end{pmatrix}, \tag{22}$$

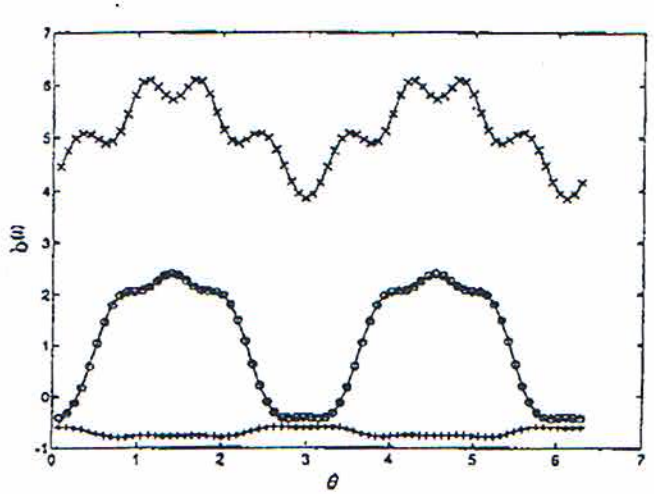

FIG. 11. The coefficients $b^{(i)}$, $i=0,1,2$, denoted by +, ∘, and ×, respectively, versus θ for $T=0.11$ and $\rho=2.8\times10^5$. The solid curves through the data points are given by Eq. (21).

and let $\tau^{(k)**}(\rho,T)$ be defined in a similar way by replacing $\tilde{f}^{(1)*}$ by $\tilde{f}^{(1)**}$ in Eq. (22). The integrations in Eq. (22) are over all values of v (where $v\geq0$) and θ. The values of $\tau^{(k)*}$ and $\tau^{(k)**}$ can also be compared to the value of $\tau^{(k)}(\rho,T)$, i.e. the stress tensor that is obtained directly from numerical data.

Figure 13 shows the traces of $\tau^{(k)}$, $\tau^{(k)*}$, and $\tau^{(k)**}$ vs T at fixed ρ. The value of $\mathrm{Tr}(\tau^{(k)*})$ is seen to be very close to $\mathrm{Tr}(\tau^{(k)})$, the discrepancy between the two values being less than 1%. This should obviously be so since the comparison is made between the data (as represented by $\tau^{(k)}$ after coarse-graining) and a best possible functional fit (i.e., $\tau^{(k)*}$) that is not subject to any phenomenological constraint. When $\tau^{(k)**}$, which is computed from a physically plausible form for $\tilde{f}^{(1)}$ given by Eq. (20), is compared to $\tau^{(k)}$, the discrepancy is found to be about 5%. This discrepancy appears to be of a systematic nature and is due to the fact that for large values of v, $\tilde{f}^{(1)**}$ underestimates $\tilde{f}^{(1)*}$.

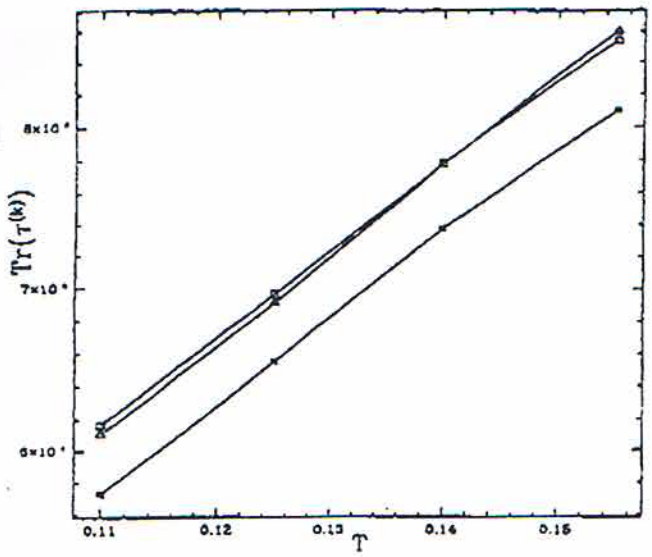

FIG. 13. Comparison of $\mathrm{Tr}(\mathcal{T}^{(1)})$, $\mathrm{Tr}(\mathcal{T}^{(1)*})$, and $\mathrm{Tr}(\mathcal{T}^{(1)**})$, corresponding to the points △, □, and □, respectively, for $T=0.11$ and $\rho=2.8\times10^5$.

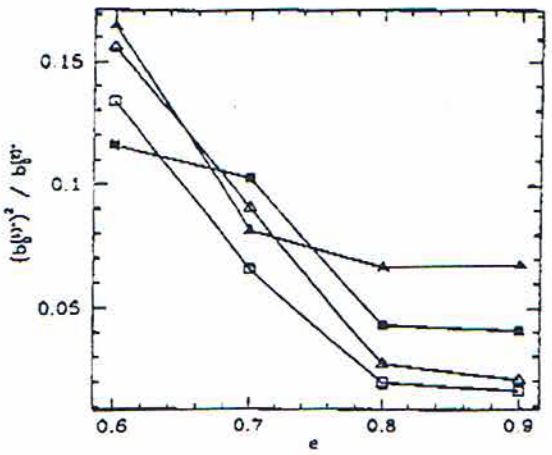

FIG. 15. The dimensionless ratio $(b_0^{(1)*})^2/b_0^{(2)*}$ vs $\tilde{e}$. For each $\tilde{e}$, this ratio is computed for different values of ρ (where $\rho=1.6\times10^5$/unit area, 2.0×10^5/unit area, 2.4×10^5/unit area, and 2.8×10^5/unit area, corresponding to the points ▲, ■, △, and □, respectively) and for the value of T that corresponds to the average temperature in the system with the given value of $\tilde{e}$. The external parameters other than $\tilde{e}$ are the same as those of System 1.

IV. FORM AND PARAMETER DEPENDENCE OF THE DISTRIBUTION FUNCTION

The accuracy of the fit for f_1 obtained in Sec. III depends on the amount of statistics collected: the more particles used in the simulation and the more configurations analyzed, the better the fit. The parametric dependence can be determined, for example, by expanding $b_{2j}^{(i)*}$ for each i nd each j in powers of T with coefficients that depend on ρ and $\tilde{e}$, and then determining these coefficients by fitting the data. Since the variation of T in the flow for $\tilde{e}$ not too close to zero is not large, a linear or quadratic dependence in T may be sufficient for the fit. We have found that linear fits are sufficient for the cases of $b_0^{(i)*}$ vs T (Fig. 12) and for $b_0^{(i)*}$ vs ρ (Fig. 14). The dependence of the amplitudes $b_{2j}^{(i)*}$ for $j>0$ (i.e., the amplitudes beyond the zeroth order) on the parameters of the problem is more complex than that of $b_0^{(i)*}$ and will not be presented here.

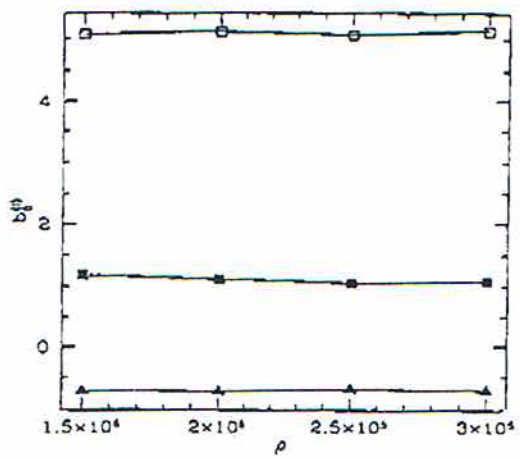

FIG. 14. Nondimensionalized zeroth-order amplitudes, $b_0^{(0)}$, $\sqrt{2T}b_0^{(1)}$, and $2Tb_0^{(2)}$, corresponding to ▲, ■ and □, respectively, versus ρ for $T=0.11$.

Figure 15 depicts the dimensionless ratio $(b_0^{(1)*})^2/b_0^{(2)*}$ vs $\tilde{e}$ for several values of ρ and for a fixed value of T that corresponds to the average temperature in the system (characterized by the given value of $\tilde{e}$). Figure 15 indicates that, relative to the size of the quadratic coefficient, $b_0^{(2)*}$, the size of the linear coefficient, $b_0^{(1)*}$, is larger, the smaller $\tilde{e}$; it decreases as $\tilde{e}$ increases and it tends to zero as $\tilde{e}$ approaches the value 1, as one expects in the elastic limit. When $\tilde{e}$ is not close to unity and the flow is highly inhomogeneous, regions with different characteristic values of the fluctuating speed coexist in the same statistical steady state (in "dynamic equilibrium") and therefore the difference between the values of $b^{(1)}$ corresponding to these regions can be large. The amplitudes of the higher harmonics in $b^{(i)}$, $i=0,1,2,$-also increase as $\tilde{e}$ becomes smaller, indicating that the flow is more anisotropic as well. These higher harmonics disappear as $\tilde{e}$ tends to 1.

V. CONCLUSION

The form of $f^{(1)}$ obtained in this work is significantly different from the ones assumed in existing kinetic theories of granular flows. These distributions are analytic in the Cartesian components of the velocity and have simple angular dependences. The form of $f^{(1)}$, which we have determined, is both nonanalytic in these components and highly anisotropic. Specifically, this form, while not containing, in the exponent, powers of the fluctuating speed, v, beyond the second (as in previous results), does contain a linear power of v. The linear power renders the function nonanalytic in the Cartesian components of v. Moreover, the magnitude of the linear coefficient, $b^{(1)}$, in highly inelastic systems is of the same order as that of the quadratic coefficient, $b^{(2)}$, though it is still

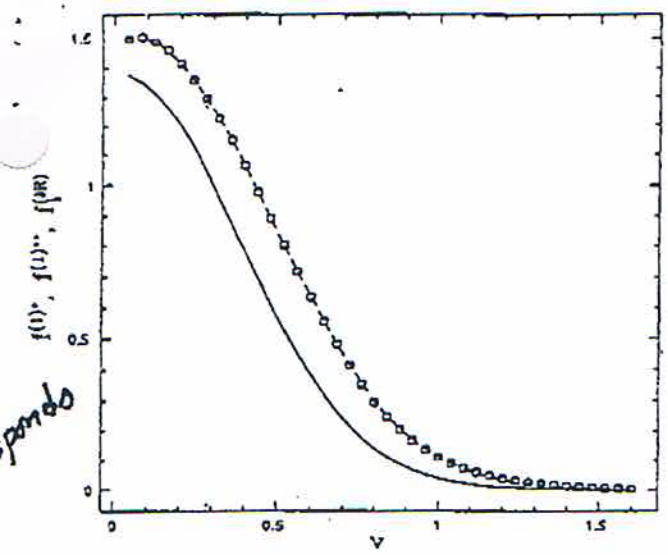

FIG. 16. The generalized Gaussian distribution for dilute shear flow, $f_1^{(JR)}$, vs $f^{(1)*}$ and $f^{(1)**}$. The □ points correspond to $f^{(1)*}$, while the dashed line corresponds to $f^{(1)**}$ and the solid line to $f_1^{(JR)}$. All distributions are shown versus v at fixed $\theta=\pi$ and $T=0.11$.

smaller in size in general. Each of the coefficients $b^{(i)}$, $i=0,1,2$, contains a finite number of non-negligible Fourier components implying a rather complicated angular dependence in $f^{(1)}$.

A comparison of $f^{(1)}$ with the distribution function for homogeneous shear flows derived by Jenkins and Richman,[10] who assumed a generalized Gaussian form, is given in Fig. and Fig. 17. The two-dimensional generalized Gaussian ("anisotropic Maxwellian") form is

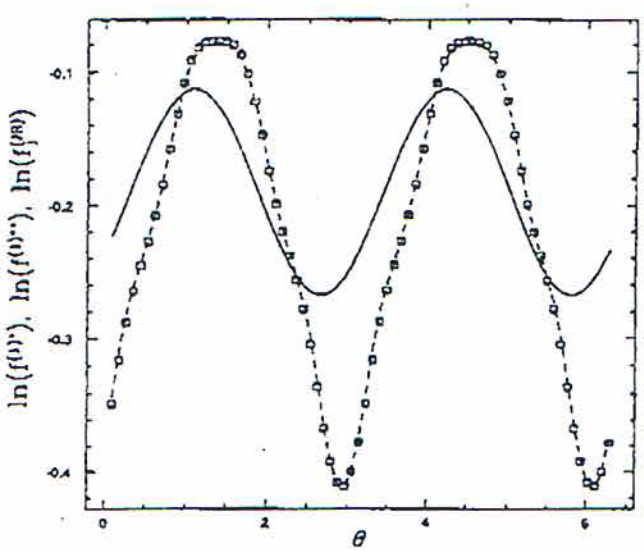

FIG. 17. The generalized Gaussian distribution for dilute shear flow, $f_1^{(JR)}$, vs $f^{(1)*}$ and $f^{(1)**}$. The □ points correspond to $f^{(1)*}$, while the dashed line corresponds to $f^{(1)**}$ and the solid line to $f_1^{(JR)}$. All distributions are shown versus θ at fixed $v=1.6$ and $T=0.11$.

$$f_1^{(JR)}=\frac{\rho}{2\pi\sqrt{\det K}}\exp\left(-\frac{1}{2}\,\mathbf{v}\cdot\mathbf{K}^{-1}\cdot\mathbf{v}\right). \tag{23}$$

where the velocity fluctuation tensor ("Reynolds stress"), $\mathbf{K}$, is given by

$$\rho\mathbf{K}\equiv\int_{\mathbf{v}}\mathbf{v}\mathbf{v}f_1^{(JR)}\,d\mathbf{v}. \tag{24}$$

In the dilute limit of the generalized Gaussian theory for shear flow $f_1^{(JR)}$ assumes the form

$$\log f_1^{(JR)}\propto-\frac{v^2}{\tilde{T}}\left[1+A^2+A\sqrt{1+A^2}\,\sin(2\theta+\chi)\right]. \tag{25}$$

where $\chi=-\tan^{-1}(A)$, and A depends, in this limit, on $\tilde{e}$ only. Thus, $\log f_1^{(JR)}$ contains only a single harmonic in θ with a phase shift χ that depends on $\tilde{e}$ only. The results presented in this section suggest that the actual single-particle distribution function has a much richer structure.

ACKNOWLEDGMENTS

It is our pleasure to acknowledge the partial support of the U.S.-Israel Binational Science Foundation, the National Science Foundation, the Advanced Research Projects Agency, and the Office of Naval Research.

[1] C. S. Campbell, "Rapid granular flows," Annu. Rev. Fluid Mech. 22, 57 (1990).
[2] H. M. Jaeger and S. R. Nagel, "Physics of the granular state," Science 255, 1523 (1992).
[3] S. R. Nagel, "Instabilities in a sand pile," Rev. Mod. Phys. 64, 321 (1992).
[4] R. P. Behringer, "The dynamics of flowing sand," Nonlinear Sci. Today 3, 1 (1993).
[5] K. Hutter and K. R. Rajagopal, "On flows of granular materials," Continuum Mech. Thermodyn. 6, 81 (1994).
[6] O. R. Walton and R. L. Braun, "Viscosity and temperature calculations for shearing assemblies of inelastic, frictional disks," J. Rheol. 30, 949 (1986).
[7] O. R. Walton and R. L. Braun, "Stress calculations for assemblies of inelastic spheres in uniform shear," Acta Mech. 63, 73 (1986).
[8] C. S. Campbell and A. Gong, "The stress tensor in a two-dimensional granular shear flow," J. Fluid Mech. 164, 107 (1986).
[9] C. S. Campbell, "The stress tensor for simple shear flows of a granular material," J. Fluid Mech. 203, 449 (1989).
[10] J. T. Jenkins and M. W. Richman, "Plane simple shear of smooth inelastic circular disks: The anisotropy of the second moment in the dilute and dense limits," J. Fluid Mech. 192, 313 (1988).
[11] M. A. Hopkins and M. Y. Louge, "Inelastic microstructure in rapid granular flows of smooth disks," Phys. Fluids A 3, 47 (1991).
[12] I. Goldhirsch and G. Zanetti, "Clustering instability in dissipative gases," Phys. Rev. Lett. 70, 1619 (1993).
[13] I. Goldhirsch, M-L. Tan, and G. Zanetti, "A molecular dynamical study of granular fluids I: The unforced granular gas dimensions," J. Sci. Comput. 8, 1 (1993).
[14] N. Sela and I. Goldhirsch, "Hydrodynamics of a one dimensional granular medium," Phys. Fluids 7, 507 (1995).
[15] M-L. Tan, "Microstructures and macrostructures in granular shear flows," Ph.D. thesis, Princeton University, 1995.
[16] M-L. Tan and I. Goldhirsch, "Intercluster interactions in rapid granular shear flows," submitted to Phys. Fluids. 1996 (in press).
[17] P. C. Johnson, P. Nott, and R. Jackson, "Frictional-collisional equations of motion of particulate flows and their applications to chutes," J. Fluid Mech., 210, 501 (1990).
[18] S. McNamara and W. R. Young, "Inelastic collapse and clumping in a one-dimensional granular medium," Phys. Fluids A 4, 496 (1992).
[19] S. McNamara and W. R. Young, "Kinetics of a one dimensional granular

corresponds.

medium in the quasielastic limit," Phys. Fluids A 5, 34 (1993).
[20]S. McNamara, "Inelastic collapse in two dimensions," Phys. Rev. E 50, R28 (1994).
[21]P. K. Haff, "Grain flow as a fluid-mechanical phenomenon," J. Fluid Mech. 134, 401 (1983).
[22]P. C. Johnson and R. Jackson, "Frictional-collisional constitutive relations for granular materials with applications to plane shearing," J. Fluid Mech. 176, 67 (1987).
[23]M. A. Goodman and S. C. Cowin, "A continuum theory for granular materials," Arch. Rat. Mech. Anal. 44, 249 (1972).
[24]J. T. Jenkins and M. W. Richman, "Grad's 13-moment system for a dense gas of inelastic spheres," Arch. Rat. Mech. Anal. 87, 355 (1985).
[25]J. T. Jenkins and M. W. Richman, "Kinetic theory for plane flows of a dense gas of identical, rough, inelastic, circular disks," Phys. Fluids. 28, 3485 (1985).
[26]C. K. K. Lun, S. B. Savage, D. J. Jeffrey, and N. Chepurnyi, "Kinetic theories of granular flow: Inelastic particles in a Couette flow and slightly inelastic particles in a general flow field, J. Fluid Mech. 140, 223 (1984).
[27]C. K. K. Lun and S. B. Savage, "A simple kinetic theory for granular flow of rough inelastic spherical particles," J. Appl. Mech. 154, 47 (1987).
[28]C. K. K. Lun, "Kinetic theory for granular flow of dense, slightly inelastic, slightly rough spheres," J. Fluid Mech. 223, 539 (1991).
[29]A. Goldshtein and M. Shapiro, "Mechanics of collisional motion of granular materials. Part 1. General hydrodynamic equations," J. Fluid Mech. 282, 75 (1995).
[30]P. Goldreich and S. Tremaine, "The velocity dispersion in Saturn's rings," Icarus, 34, 227 (1978).
[31]R. J. Boyle and M. Massoudi, "A theory for granular materials exhibiting normal stress effects based on Enskog's dense gas theory," Int. J. Eng. Sci. 28, 1261 (1990).
[32]I. Goldhirsch and N. Sela, "Generic nature of normal stress differences in granular and molecular sheared fluids," submitted to Phys. Rev. Lett.
[33]S. Chapman and T. G. Cowling, *The Mathematical Theory of Nonuniform Gases*, 3rd ed. (Cambridge University Press, 1970).
[34]M. A. Hopkins and H. H. Shen, "A Monte-Carlo solution for rapidly shearing granular flows based on kinetic theory of dense gases," J. Fluid Mech. 244, 477 (1992).
[35]A. W. Lees and S. F. Edwards, "The computer study of transport processes under extreme conditions," J. Phys. C. Solid Phys. 5, 1921 (1972).
[36]Y. H. Taguchi and N. Takayasu, "A set of hard spheres with tangential inelastic collisions as a model of granular matter: $1/f^{\alpha}$ fluctuations, non-Gaussian distribution and convective motion," submitted to Phys. Rev. Lett.
[37]Y. H. Taguchi, "Turbulent nature of powder flow in vibrated bed: Numerical study," Am. Soc. Mech. Eng. NY 185, 251 (1994).
[38]J. T. Jenkins, "Boundary conditions for rapid granular flow: Flat, frictional walls, Trans. ASME: J. Appl. Mech. 59, 120 (1992).
[39]J. W. Duffy, J. J. Brey, and A. Santos, "Some theoretical aspects of nonequilibrium simulation methods," in *Molecular-Dynamics Simulation of Statistical-Mechanical Systems: Varenna on Lake Como*, Villa Monastero, 23 July–2 August 1985, 1986, p294–303.
[40]D. C. Rapaport, "The event scheduling problem in molecular dynamics simulation," J. Comput. Phys. 34, 184 (1980).

H. Takayasu

reference 32 should read:

I. GOLDHIRSCH AND N. SELA, "ORIGIN OF NORMAL STRESS DIFFERENCES IN RAPID GRANULAR FLOWS", submitted to Phys. Rev. Lett.